Renewable Energy 45 (2012) 96–110

Contents lists available at SciVerse ScienceDirect

Renewable Energy

journal homepage: www.elsevier.com/locate/renene

Control strategy for distributed integration of photovoltaic and energy storage systems in DC micro-grids

N. Eghtedarpour, E. Farjah*

School of Electrical & Computer Engineering, Shiraz University, Shiraz, Fars, Iran

ARTICLE INFO

Article history:
Received 18 October 2011
Accepted 22 February 2012
Available online 24 March 2012

Keywords:
Micro-grid
Renewable energy
PV
Battery energy storage

ABSTRACT

The interest on DC micro-grid has increased extensively for the more efficient connection with DC output type sources such as photovoltaic (PV) systems, fuel cells (FC) and battery energy storage systems (BESS). Furthermore, if loads in the system are supplied with DC power, the conversion losses from sources to loads are reduced compared with AC micro-grid. This paper proposes operation and control strategies for the integration of PV and BESS in a DC micro-grid. The proposed control enables the maximum renewable energy utilization during different operating modes of the micro-grid i.e., grid connected, islanded or transition between these two modes, whilst making an allowance for the DC voltage control and DC-loads supply. When the system is grid connected and during normal operation, active power is balanced by the AC grid converter to ensure a constant DC voltage. In order to achieve the system operation under islanding conditions, a coordinated strategy for the BESS, PV and load management including load shedding and considering battery state of charge (SoC), are proposed. Seamless transition of the PV converter control between maximum power point tracking (MPPT) and voltage control modes, of the battery converter between charging and discharging and that of grid side converter between rectification and inversion are ensured for different grid operation modes by the proposed control methods. The DC bus voltage level is employed as an information carrier to distinguish different modes and determine mode switching. MATLAB/SIMULINK simulations are presented to demonstrate the robust operation performance and to validate the proposed control system during various operating conditions.

1. Introduction

Renewable energy emerges as an alternative way of generating clean energy. Recent advances using smart micro-grids to maximize operations efficiency and reliability have made this kind of systems a suitable solution for decentralizing the electricity production.

In the view of the fact that most renewable energy sources (RES), such as photovoltaic, fuel cells and variable speed wind power systems generate either DC or variable frequency/voltage AC power; a power–electronics interface is an indispensable element for the grid integration [1,2]. In addition, modern electronic loads such as computers, plug-in hybrid electric vehicles and even traditional AC loads such as induction motors, when driven by a variable speed drive; require DC power. DC micro-grids have shown advantages in terms of efficiency, cost and system that can eliminate the DC–AC or AC–DC power conversion stages required in AC micro-grids for the integration of mentioned renewable energy sources and loads. Typical examples of DC micro-grids are power systems in commercial centers containing sensitive loads [3], industrial [4], shipboard [5] and vehicular and more electric aircraft [6] power systems. Due to nondeterministic characteristic of RES, energy storages (ES) are requisite for consistent operation of standalone renewable systems. In these systems, ES is responsible for balancing short term differences between the source and load power due to stochastic variations of renewable energy. A supervisory power management strategy is also necessary in order to maximize the use of renewable energy.

Most of the research conducted so far has focused on the control, operation and power sharing of DGs in an AC micro-grid during and subsequent to islanding [7–10]. Recently, some researches have also been carried out on DC micro-grids. Ref. [11] presents a low-voltage DC micro-grid for supplying a residential complex. Super capacitors are exploited as the main ES for supplying sensitive loads during disturbances. The generations and ES in the DC micro-grid have been assumed to be large enough to supply the full load demand which guarantees a seamless transfer between different system operating modes including islanding

* Corresponding author.
E-mail address: farjah@shirazu.ac.ir (E. Farjah).

0960-1481/$ – see front matter © 2012 Elsevier Ltd. All rights reserved.
doi:10.1016/j.renene.2012.02.017

Nomenclature

PV parameters

i_{pv}, v_{pv}	PV output current and voltage
P_{pv}	PV system output power
R_s	Series resistance representing the structural resistances
R_p	Parallel resistance modeling the leakage current
a	Diode ideality factor representing the recombination effect in the space-charge region of PV
I_0	Diode reverse saturation current
M_s	Number of series connected PV cells in a PV module
k	Boltzmann's constant
q	Electron charge
K	Polarization voltage
N_p	Number of parallel-connected PV cells
N_s	Number of series connected PV cells
I_d	Diode current in the equivalent circuit of PV cell
I_i	Terminal current of the ideal PV module
V_{pv}^{ref}	Reference voltage command for input voltage of PV converter
V_{MPP}^{ref}	Reference voltage for MPPT in PV converter
V_{VC}^{ref}	Reference voltage for output voltage control in PV converter

GS-VSC parameters

P_{grid}	GS-VSC power
P_{load}	DC load power
V_{grid}	Grid voltage
I_{DC}^{grid}	Current in DC side of the GS-VSC
V_{grid}^{ov}	Grid overvoltage level
P_{dc}, P_{ac}	Power on DC and AC sides of the GS-VSC
C	DC-link capacitance
V_{DC}	DC-link voltage
V_{vsc}	Reference voltage for the GS-VSC
V_{shed}	Reference voltage for the load shedding

Battery parameters

R_{batt}	Resistance that the battery opposes to the flow of energy
I_{batt}	Battery current
V_{batt}	Battery output voltage
P_{BESS}	BESS output power
E_{g0}	Constant voltage of the battery
Q	Battery capacity
A, B	Exponential voltage and exponential capacity in the battery model
SoC	State of charge of the battery
η_c	Charging efficiency of the battery
$C_{nominal}$	Rated battery capacity (at n hours)
$C_{t\ coef}$, A_{cap}, B_{cap}	Constants in battery model
ΔT	Temperature variation from the reference value of 25 °C
$I_{nominal}$	Discharge current corresponding to $C_{nominal}$ rated capacity
α, β	Temperature coefficients in battery model
V_{ref}^{batt}	Reference voltage for BESS
ΔV^{-}	Reference voltage for the BESS to start discharging
ΔV^{+}	Reference voltage for the BESS to start charging

DC/DC converters parameter

d	Switch duty cycle
C	Input filter capacitance of PV converter
v_C	Voltage across C
C_o	Converter output filter capacitor
R_o	Capacitor equivalent series resistance
L	Converter input filter inductance
R_L	Equivalent series resistance of input filter inductor
i_L	Input filter inductor current
v_{C_o}	Voltage across C_o
i_o, v_o	Converter output current and voltage

operation. However, in a renewable based micro-grid this cannot be assured because of nondeterministic generation characteristics and requires more careful management and control between the sources and loads during different disturbances. A distributed DC power system with multiple RES and loads is proposed in [12]. The main issue investigated is the DC bus voltage control and power sharing when applied to a wind powered system. However, only the autonomous operation of the DC micro-grid is inspected. Operational analysis of a bus type DC micro-grid is also presented in [13] considering different RES, but the power management scheme for RES is not presented. Ref. [14] also proposes a control strategy for a DC distribution system for the stable operation of wind generation under the line-fault using the BESS.

Employment of PV generation in DC systems has been paid more attention in recent years. Ref. [15] describes operation of an isolated DC grid including PV as the main renewable source and battery energy storage to supply unbalanced AC loads. However, the grid connection mode and the transition to islanding are not considered. In [16] a standalone DC grid with PV, FC and BESS interconnection is presented and a distributed DC bus voltage control is investigated for various working states of the system. But, connection to the grid and islanding transients is not considered. Output voltage control of a PV DC/DC boost converter in an isolated DC distribution system is proposed in [17]. Variation of the PV voltage is considered in the DC bus voltage control scheme. However, a full consideration of the system transients, ES and grid connection states are not studied. In [18–21] PV based standalone DC micro-grid utilizing active power management strategies are developed for supplying small residential loads. In these systems, the SoC limits of batteries are regarded, but grid connected power flow is not taken into account.

Another issue to be regarded is the micro-grid power management. Similar to an AC micro-grid, a proper power management system is required for a reliable operation of renewable sources and energy storages in a DC micro-grid, apart from the micro-grid mode of operation, [22]. In the grid connected mode, RES are expected to work in MPPT and deliver the maximum available power to the grid. The utility grid is expected to support the balance of power and regulate the DC voltage. In the autonomous mode of operation, the available power of the RES units must meet the total load demand of the micro-grid; otherwise, the ES is required to supply the difference and in case of insufficient storage the system must undergo load shedding to match generation and load demand. In addition, fast and flexible DC voltage control strategies are required to minimize the micro-grid dynamics. Active power management scheme has been widely utilized for the integration of RES and ESS to the DC bus [18–21,23–26]. However, in a DC micro-grid DGs are usually dispersed throughout the grid and active power management scheme requests a communication link which is not greatly accepted. On the other hand, distributed power management systems have shown to be more reliable for micro-grid management and can be implemented devoid of a communication link [27]. A distributed control strategy known as "DC-Bus signaling

(DBS)" has been proposed and applied to a hybrid renewable standalone nano-grid [28]. In this approach DC bus voltage level change is utilized as a communication link between sources and storages. However, the AC grid interface and restrictions usually occurred in a micro-grid are not included in [28].

In this paper, a new system operation and control strategy is proposed for the distributed integration of PV and BESS in a DC micro-grid. The proposed control enables the maximum renewable energy utilization during different operating modes of the micro-grid, whilst considering the DC voltage control, battery power limitation, battery SoC and DC-loads supply. The control strategies do not include any hysteresis for switching between operating modes which enables a seamless operation of the micro-grid in different operating modes. A distributed power management system based on modified DBS (MDBS) is utilized for the control of PV and ES systems throughout the grid. DC micro-grid configuration and the operation scenarios are described in Section 2. In Section 3, the system modeling and the proposed system control strategies are discussed. The DC micro-grid power management scheme is presented in Section 4. The effectiveness of the proposed system and control strategies is validated by SIMULINK/MATLAB simulations and results are shown in Section 5 and finally the conclusion is given in Section 6.

2. System configuration and operation

2.1. DC micro-grid structure and circuit configuration

The investigated DC micro-grid layout is shown in Fig. 1. The system consists of a PV source connected through a DC/DC boost converter and a battery energy storage, which is connected through a bi-directional buck-boost DC/DC converter. The BESS is utilized to balance the power difference between the PV power supply and load demand in islanding mode. A bi-directional DC/AC converter called GS-VSC is also used to connect the DC bus and AC main grid, which enables bi-directional power flow. PV and BESS are at different location in the system therefore a decentralized control strategy based on MDBS is considered for the coordination of PV and BESS in the system. The primary source of power generation for the DC micro-grid is the PV system, which is controlled to operate at MPPT. The battery meets the sensitive load demand to maintain a continuous supply of power in case of fluctuations in the main grid or during islanding operation.

2.2. Grid operating modes

DC micro-grid should operate in both grid connected and islanding states. In each of these two states, there are different operating modes and the control and management system should regulate the DC bus voltage. Different operating modes are considered for the DC micro-grid, which are summarized in Table 1. In Mode I, the DC micro-grid is connected to the grid and operating under light load condition. The PV is working in MPPT and BESS in charging or off state while the DC bus voltage is controlled by the GS-VSC and surplus power generated by the PV is delivered to the main grid. Operating Mode II usually occurs during heavy load. PV and BESS states are the same as Mode I but the insufficient power is supplied by the GS-VSC. Mode III and IV correspond to the islanding state of the micro-grid where the PV is operating in MPPT and the insufficient/surplus power is balanced by discharging/charging of the BESS. In these two modes, the storage system is responsible for voltage regulation. Mode V refers to the case where the BESS is fully charged in the islanded micro-grid and the demanded power is less than maximum power of the PV system. In this case, in order to protect the battery from overcharging the PV should be capable to control the output power and regulate the DC voltage by working in off-MPPT state. In Mode VI, the micro-grid is also in islanding state and the required power is larger than the total maximum power of PV and BESS. Consequently, in order to maintain the system stability load shedding is required.

Table 1
DC micro-grid operating modes.

Mode	Micro-grid state	PV state	BESS state	GS-VSC
I	Grid connected	MPPT	Charging/off	Inverting mode
II	Grid connected	MPPT	Charging/off	Rectifying mode
III	Islanding	MPPT	Discharging/off	Disconnected
IV	Islanding	MPPT	Charging/off	Disconnected
V	Islanding	Off-MPPT	Off	Disconnected
VI	Islanding	MPPT	Limited	Disconnected

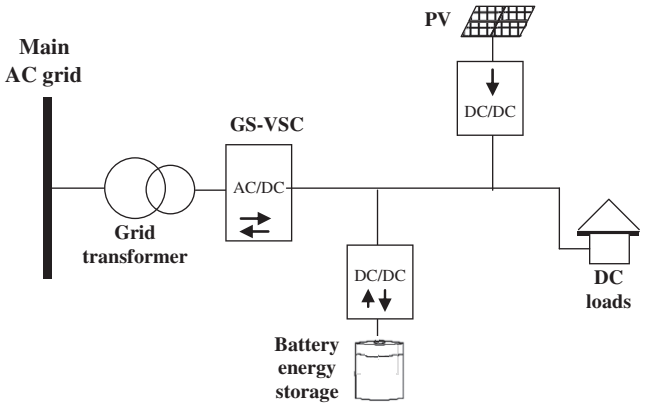

Fig. 1. The layout of the studied DC micro-grid for the integration of PV and BESS.

3. System modeling and control

3.1. Modeling of PV system

3.1.1. PV array modeling

Since the PV characteristics can significantly influence the design and operation of power converter and the control system, a brief review of PV array modeling is presented in this section. Different equivalent circuits of a PV cell have been proposed in the literature. The single-diode circuit is the most commonly used model [29,30], since it represents a reasonably good trade-off between simplicity and accuracy. Fig. 2 shows the single-diode equivalent circuit of a PV cell. The circuit is composed of a current source, a diode in parallel with the current source, the series resistance, and the parallel resistance. The basic equation describing the nonlinear current–voltage relationship of the PV cell is [29]

$$I_{\mathrm{pv}}(V_{\mathrm{pv}}) = I_g - I_d - \left(\frac{V_{\mathrm{pv}} + R_s I_{\mathrm{pv}}}{R_p}\right)$$
$$I_d = I_0\left(e^{\frac{q(V_{\mathrm{pv}}+R_s I)}{M_s k T a}} - 1\right) \quad (1)$$

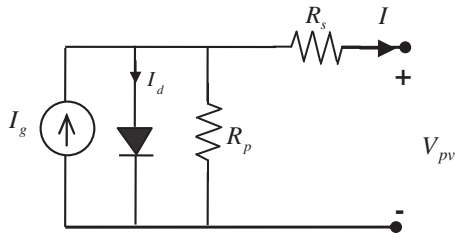

Fig. 2. Single-diode equivalent circuit of a real PV cell or module.

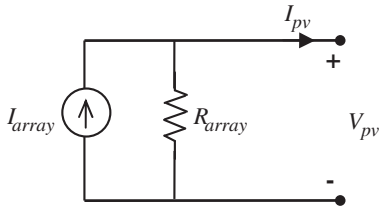

Fig. 3. Norton equivalent circuits of PV array.

the current source I_g modeling the photon-generated electron–hole pairs under the influence of the built-in field and is a function of the p–n junction temperature (T) and Solar radiation. Norton equivalent circuit of Fig. 3 is exploited to model a PV array including N_p parallel and N_s series connected PV cells. The circuit consists of the equivalent current source (I_{array}) and the equivalent resistance (R_{array}) defined as,

$$I_{\text{array}} = N_p I_i \frac{R_p}{R_p + R_s} \tag{2}$$

$$R_{\text{array}} = \frac{N_s}{N_p}(R_p + R_s) \tag{3}$$

3.1.2. PV system and its control algorithm

A boost DC/DC converter is exploited to connect the PV array to the micro-grid. The circuit diagram of the PV system is shown in Fig. 4. According to the operating modes of the micro-grid discussed in the Section 2.2, the PV should operate both in MPPT and voltage control modes. A common solution to this problem may be followed using a separate control loop for each operating mode and switch to the proper control loop that may cause some unfavorable transients in mode transitions. In a distributed power system, a mode detection procedure is also needed in order to recognize different operating conditions. A new control strategy is proposed in this section for the smooth control of the PV system in the two intended modes. The control contains no hysteretic block which enables a seamless transition between the modes while provides maximum power utilization of the PV systems.

The block diagram of the proposed control topologies for the PV system is shown in Figs. 5 and 6. The DC/DC boost converter employs the peak current-mode control (PCM) with slope compensation [31] to control the input voltage (or equally the PV array voltage). The PCM control is a two-loop control system; a voltage loop with an additional inner current loop which monitors the inductor current (or equally PV array current) and compares it with its reference value that enables overloading protection of the PV array. The reference value for the inductor current is generated by the outer voltage loop. In the proposed control strategy a combined outer voltage loop is added to the PCM

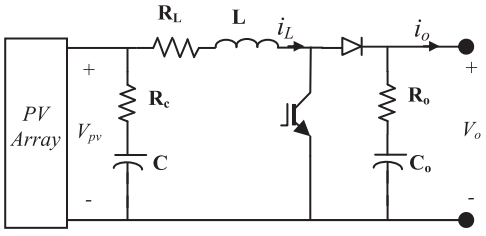

Fig. 4. Boost converter for the PV system.

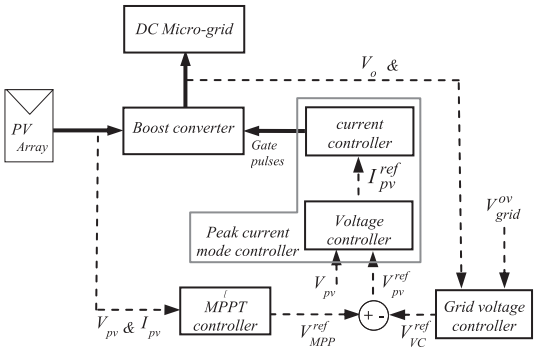

Fig. 5. Block diagram of the proposed control topologies for PV system.

controller which generates $V_{\text{pv}}^{\text{ref}}$ by means of considering both the MPPT control loop and the grid voltage control loop. Converter input voltage is controlled to get MPPT [32] or to regulate the output DC voltage when needed. A general perturbation-and-observe MPPT method [33] is implemented for the PV system in the current study. P_{pv} is calculated by measuring V_{pv} and I_{pv}. At the maximum power point (MPP), the derivative ($\text{d}P_{\text{pv}}/\text{d}V_{\text{pv}}$) is equal to zero and the maximum power point can be achieved by changing $V_{\text{MPP}}^{\text{ref}}$. On the other hand, in the grid voltage control mode the control loop shifts the $V_{\text{pv}}^{\text{ref}}$ from the MPP by controlling the$V_{\text{VC}}^{\text{ref}}$. The combination of MPPT and voltage control loops is exploited for instantaneously balancing the system power and controlling the grid voltage in required operating modes. The block diagram of the proposed grid voltage controller is shown in Fig. 6. In the grid connected mode, the power balancing and voltage regulation is prepared by the GS-VSC, hence V_{grid} is below $V_{\text{grid}}^{\text{ov}}$ and the grid voltage control loop is disabled by the positive limiter block. Therefore, PV will operate in MPPT mode. Operating modes of the PV, GS-VSC and battery in this case are shown schematically in Fig. 7 (a) for Mode I and Fig. 7 (b) for Mode II of operation. During islanding state, based on the PV power generation, the battery maximum power, SoC of the battery and the load condition, the designed controller can control the PV system in three operating modes, as shown in Fig. 8. Fig. 8 (a) shows the Mode III where the available maximum PV power is less than the demanded load power. The insufficient power will be supplied by controlling the discharge of the battery as will be discussed in the next section. On the other hand, when the available maximum discharge power of the battery is less than the demanded power, a load shedding system will trip the required amount of the load to avoid over-discharge of the battery. Fig. 8 (b) shows the Mode IV in which the available maximum power of PV is larger than the load power and the excessive power will charge the battery, but the charging current is less than the nominal charging current of the battery. In this case, the PV operates in MPPT mode, the battery regulates the grid voltage by absorbing the surplus power, and the battery is partially charged in constant voltage mode. When the available maximum power of the PV is larger than the battery charging and load demand, the DC voltage increases. As the grid voltage reaches $V_{\text{grid}}^{\text{ov}}$, the signal generated by the voltage control loop in Fig. 6 is actuated and shifts the PV voltage to off-MPPT as shown in Fig. 8 (c).

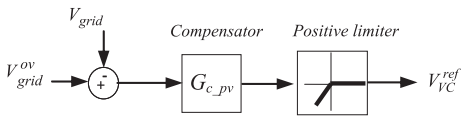

Fig. 6. Block diagram of the grid voltage control.

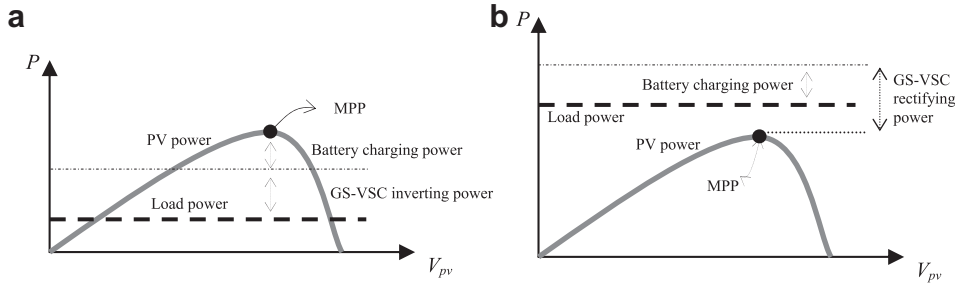

Fig. 7. Operation modes of the PV, GS-VSC and battery connected to the main grid (a) PV in MPPT and battery in charging, GS-VSC in inverting mode. (b) PV in MPPT and battery in charging, GS-VSC in rectifying mode.

In this case, the PV system operates in voltage control mode and balances the power in the micro-grid.

Through the planned power arrangement scheme, the PV module will operate at MPPT, and the MPPT is discarded merely when the PV power is larger than the total demanded power for battery charging and load supplying, hence a seamless transfer between MPPT and voltage control modes is conducted and there is no need for hysteretic control schemes.

3.1.3. Small signal modeling of PV system

Due to nonlinear characteristic of PV array, a linear PV model is necessary for the small signal analysis and controller design. The *I–V* curve of a typical photovoltaic output is shown in Fig. 9. According to the operating point of the PV, the curve can be divided into four regions: 1) the current source region; 2) power region I; 3) power region II; and 4) the voltage source region [32]. The derivative of the nonlinear model of PV at a given (*V*, *I*) point can be presented as,

$$g(V,I) = \left.\frac{\partial i_{\mathrm{pv}}}{\partial v_{\mathrm{pv}}}\right|_{(V,I)} = -\frac{A_0 + 1/R_p}{1 + R_s/R_p + R_s A_0} \tag{4}$$

where

$$A_0 = I_0\left(\frac{q\, e^{\frac{q(V+R_s I)}{M_s kTa}}}{M_s kTa}\right) \tag{5}$$

The PV model can be rewritten as

$$i_{\mathrm{pv}}(t) = g(V,I)v_{\mathrm{pv}}(t) \tag{6}$$

Linearizing Equation (4) using Perturbation and Linearization method leads to the following linearized model of PV

$$I_{\mathrm{pv}} + \hat{i}_{\mathrm{pv}} = g(V,I)(V_{\mathrm{pv}} + \hat{v}_{\mathrm{pv}}) \tag{7}$$

$$\hat{v}_{\mathrm{pv}} = V_{\mathrm{pv}}^{\mathrm{eq}} - R_{\mathrm{pv}}^{\mathrm{eq}}\,\hat{i}_{\mathrm{pv}} \tag{8}$$

$$V_{\mathrm{pv}}^{\mathrm{eq}} = -V_{\mathrm{pv}} + \frac{I_{\mathrm{pv}}}{g}, R_{\mathrm{pv}}^{\mathrm{eq}} = -\frac{1}{g} \tag{9}$$

Equation (6) describes the linearized Thevenin model of the circuit of Fig. 3.

The slope of the curve is big in voltage source region and gets smaller in the current source region. This slope is proportional to dynamic resistance and the operating condition can consequently affect the system dynamics. It is shown in [32] that the operation in the current source region of the *I–V* curve presents the worst and most critical dynamic behavior therefore the controller is designed considering this operating point.

According to Fig. 4, the boost converter is described by the following nonlinear state-space-averaged equations [31]

$$\frac{\mathrm{d}i_L}{\mathrm{d}t} = -\frac{R_L}{L}i_L + \left(\frac{1-d}{L}\right)v_o + \frac{1}{L}v_{\mathrm{pv}} \tag{10}$$

$$\frac{\mathrm{d}v_c}{\mathrm{d}t} = \left(\frac{1-d}{C}\right)i_L - \frac{1}{C}i_o, v_{\mathrm{pv}} = R_c C\frac{\mathrm{d}v_c}{\mathrm{d}t} + v_c \tag{11}$$

$$\frac{\mathrm{d}v_o}{\mathrm{d}t} = \left(\frac{1-d}{C}\right)i_L - \frac{1}{C}i_o \tag{12}$$

The boost converter is intended to control the PV voltage in order to track the MPP and to regulate the DC voltage in the voltage control mode. A small signal model of the PV system with peak current-mode along with input voltage controlled boost converter can now be constructed by perturbation and linearization of Equations (6)–(9) as follows

$$\frac{\hat{v}_{\mathrm{pv}}}{\hat{i}_L} = -\frac{R_{\mathrm{pv}}^{\mathrm{eq}}(1 + R_c C\, s)}{1 + (R_{\mathrm{pv}}^{\mathrm{eq}} + R_c)C\, s} \tag{13}$$

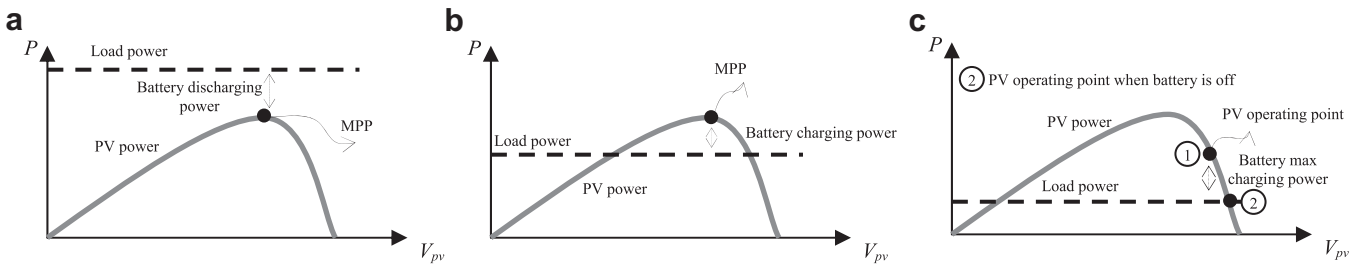

Fig. 8. Operation modes of the PV and battery in islanding state (a) PV in MPPT and battery in discharging mode. (b) PV in MPPT and battery in partial charging mode. (c) PV in voltage control mode and battery in partial charging mode.

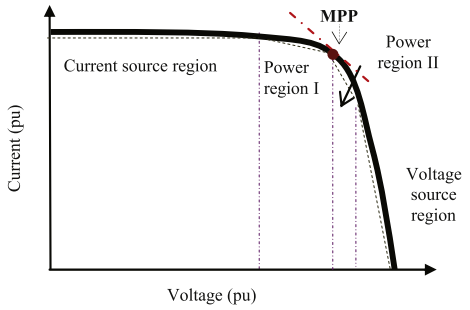

Fig. 9. Linear approximation of photovoltaic output characteristics.

$$\hat{i}_L\hat{d} = V_o \frac{1+(R_{pv}^{eq}+R_c)Cs}{s^2+\dfrac{(R_{pv}^{eq}R_cC+R_L(R_{pv}^{eq}+R_c)+L)}{(LC(R_{pv}^{eq}+R_c))}s+\dfrac{(R_{pv}^{eq}+R_L)}{(LC(R_{pv}^{eq}+R_c))}} \quad (14)$$

3.2. Modeling of BESS

3.2.1. Battery modeling

Due to the nonlinear characteristic of battery, its proper representation in the controller becomes another challenge. Different models for battery behavior simulation with different degrees of complexity and simulation behavior are available. The simplest and commonly used model of a battery contains an ideal voltage source in series with a constant internal resistance [34]. Another commonly used battery model is the Thevenin model [35], which consists of an ideal no-load battery voltage, series internal resistance in series with parallel combination of overvoltage resistance and capacitance. More realistic models have been proposed to take into account the nonlinear parameters [36]. These models characterize the battery internal resistance, self-discharge resistance, overcharge resistance; and separate the charging and discharging process. To avoid excessive complexity while considering the dynamics of the battery, a generic dynamic battery model is proposed in [37] including the battery state of charge SoC and the current flowing across the battery. The equivalent circuit model is depicted in Fig. 10 and can be described by the following equations,

$$\begin{aligned} V_{batt} &= E_g - i_{batt}R_{batt} \\ E_g &= E_{g_0} - K\frac{Q}{Q-\int i_{batt}dt} + A\exp\left(B.\int i_{batt}dt\right) \end{aligned} \quad (15)$$

The voltage source E_g represents the voltage at open circuit between the battery terminals and depends directly on the stored energy. It is shown by experimental tests that this model can sufficiently reproduce the behavior of batteries during the charge/discharge processes [35]. The state of charge of the battery can also be described by the following equations,

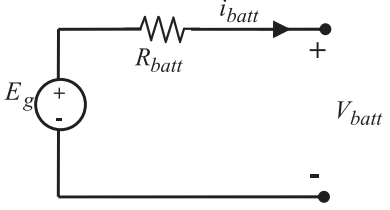

Fig. 10. Equivalent circuit for the battery.

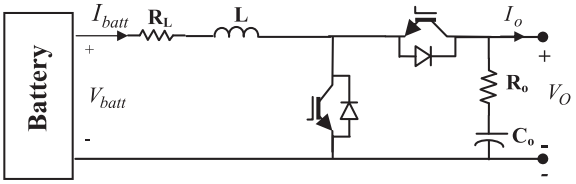

Fig. 11. Bi-directional buck-boost battery converter.

$$SoC(t_i) = \frac{1}{Q(t_i)}\int_{\infty}^{t_i}\eta_c(t)I_{batt}(t)dt$$

$$Q(t_i) = \frac{C_{nominal}C_{t\ coef}}{1+A_{cap}\left(\dfrac{|I_{batt}(t)|}{I_{nominal}}\right)^{B_{cap}}}\left(1+\alpha_c\Delta T(t)+\beta_c\Delta T^2(t)\right) \quad (16)$$

$$I_{nominal} = \frac{C_{nominal}}{n} \text{ for } n \text{ hours}$$

More details on battery modeling and coefficients can be followed in [37].

3.2.2. Control algorithm for BESS

One of the most flexible methods for the superior performance of BESS in DC grid is to connect the battery by a proper DC/DC converter [23]. A bi-directional Buck-Boost DC/DC converter shown in Fig. 11 is used in the current study. Under different micro-grid conditions, the BESS operates at charging, discharging or floating modes and the modes are managed according to the DC bus voltage condition at the point of BESS coupling. Consequently, the BESS is required to provide necessary DC voltage control under different operating modes of the micro-grid. The BESS control loops are shown in Fig. 12. The converter output voltage (or equally the grid voltage) (v_o) is compared with V_{batt}^{ref} and passes through an asymmetrical dead-zone block to control charge/discharge command for the battery and eliminate several needless charge/discharge of the battery during normal grid conditions. The dead-zone is also responsible for power sharing between multiple energy storages in the grid. When the grid voltage is in allowable range ($\Delta V^-, \Delta V^+$) the BESS is in floating state. If the grid voltage goes beyond $V_{ref}^{batt}+\Delta V^+$ the battery enters charging mode subject to the SoC limitation. In the case where the grid voltage is beneath $V_{ref}^{batt}-\Delta V^-$ and the SoC is above the minimum permissible value, the BESS operates in DC voltage control mode in order to maintain a constant DC voltage. The SoC is measured by the battery management system and disable battery charging/discharging when the SoC is in forbidden regions.

Alternatively, by regulating the slope of the dead-zone block in linear regions, it is possible to implement a voltage droop power charge/discharge sharing between different energy storage systems

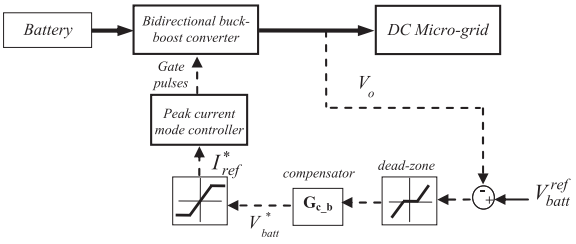

Fig. 12. Block diagram of the proposed control topologies for BESS.

throughout the grid [12]. This fact is illustrated schematically in Fig. 13.

3.2.3. Small signal modeling of BESS

Regarding the relatively large time constant of the battery, it can be modeled as a constant voltage source in small signal analysis. The average state-space model of the battery converter could be defined by the following equations

$$\frac{\mathrm{d}i_{\mathrm{batt}}}{\mathrm{d}t} = \left(\frac{1-d}{L}\right)v_o + \frac{R_L}{L}i_{\mathrm{batt}} + \frac{d}{L}V_{\mathrm{batt}} \tag{17}$$

$$\frac{\mathrm{d}v_{C_o}}{\mathrm{d}t} = \left(\frac{1-d}{C_o}\right) i_{\mathrm{batt}} - \frac{1}{C_o}i_o, v_o = R_o C_o \frac{\mathrm{d}v_{C_o}}{\mathrm{d}t} + v_{C_o} \tag{18}$$

The BESS control strategy, shown in Fig. 12, determines the proper duty cycle of the converter in order to maintain the DC bus voltage in the nominal value, while the battery voltage varies depending on the operating mode (charge or discharge) of the battery. The control-to-output transfer function of the converter can be expressed by

$$\frac{\hat{v}_o}{\hat{d}} = \frac{V_o(1-D)}{LC_o}\frac{(1+C_oR_os)}{s^2 + \dfrac{C_o\left(R_L+(1-D)^2R_o\right)}{LC_o}s + \dfrac{(1-D)^2}{LC_o}} \tag{19}$$

3.3. Grid side VSC control method

As discussed earlier, the function of GS-VSC is to regulate the DC-link voltage during grid connected mode. A two level VSC is used to link DC and AC grids. Peak current-mode control approach [31] is exploited for real/reactive power control at AC side. Thus, the amplitude and the phase angle of the VSC terminal voltage are controlled in a dq rotating reference frame. The DC-link voltage control is accomplished through the control of the real power component. DC voltage dynamics can be formulated based on the principle of power balance, as

$$\frac{\mathrm{d}}{\mathrm{d}t}\left(\frac{1}{2}C\cdot V_{\mathrm{DC}}^2\right) = P_{\mathrm{dc}} - P_{\mathrm{ac}} \tag{20}$$

$$P_{\mathrm{dc}} = V_{\mathrm{DC}}\cdot i_{\mathrm{grid}}^{\mathrm{DC}} \tag{21}$$

3.4. System voltage variation ride-through capability during transients

During transients in the micro-grid, a decrease/increase in voltage amplitude occurs. In order to control the voltage in the standard range, it is required to supply the demanded power to the micro-grid. However, the battery/PV includes an inherent time constant in order to response toward the transients. This will thus limit the power that the DC micro-grid can control to supply the load. In such cases, capacitors along the DC grid can act as a virtual inertia to supply the insufficient or absorb the surplus energy. The DC-link power balance can be expressed by the following differential equation,

$$CV_{\mathrm{DC}}\frac{\mathrm{d}V_{\mathrm{DC}}}{\mathrm{d}t} = P_{\mathrm{pv}} + P_{\mathrm{BESS}} - P_{\mathrm{load}} - P_{\mathrm{grid}} \tag{22}$$

According to the Equation (21), in order to regulate the DC-link voltage, it is necessary to keep the power balance in DC-link. In this equation, the change in grid power is considered as disturbance during the transients. Moreover, to meet the power balance in DC-link, it is important to consider the dynamic limitations of the BESS; the battery power could not change rapidly however, the amount of power that should be delivered by the system equivalent capacitor (C) to balance the power in DC-link is very important and it depends on the DC-link energy. Considering the minimum/maximum acceptable DC-link voltage ($V_{\mathrm{DC}}^{\min}/V_{\mathrm{DC}}^{\max}$) and the battery reference voltage for charge ($V_{\mathrm{charging}} = V_{\mathrm{ref}}^{\mathrm{batt}} + \Delta V^+$) and discharge ($V_{\mathrm{discharging}} = V_{\mathrm{ref}}^{\mathrm{batt}} - \Delta V^-$) the energy to be delivered to or absorbed from the grid can be expressed by means of the following calculation:

$$\Delta E_c = \frac{1}{2}C\left(V_{\mathrm{discharging}}^2 - V_{\mathrm{DC}}^{2\min}\right) \text{ for voltage drop} \tag{23}$$

$$\Delta E_c = \frac{1}{2}C\left(V_{\mathrm{charging}}^2 - V_{\mathrm{DC}}^{2\max}\right) \text{ for voltage rise} \tag{24}$$

Then regarding the unbalanced power (P_{unbal}), the time constant of the BESS should be at least,

$$\tau = \frac{\Delta E_c}{P_{\mathrm{unbal}}}(\mathrm{s}) \tag{25}$$

One of the solutions to mitigate the dependency on the system capacitance is by using fast energy storage systems such as super capacitors as shown in [24].

The above discussion can also be extended to the disturbances such as fault on the AC grid and the corresponding transients on the DC micro-grid.

Table 2
Voltage levels for recognizing different operating modes.

Operating mode	DC-link voltage
Mode I, II	$V_{\mathrm{ref}}^{\mathrm{batt}} + \Delta V^+ < V_{\mathrm{dc}} \le V_{\mathrm{grid}}^{\mathrm{ov}}$
Mode III	$V_{\mathrm{dc}} \ge V_{\mathrm{ref}}^{\mathrm{batt}} + \Delta V^+$
Mode IV	$V_{\mathrm{dc}} \le V_{\mathrm{ref}}^{\mathrm{batt}} - \Delta V^-$
Mode V	$V_{\mathrm{dc}} \ge V_{\mathrm{grid}}^{\mathrm{ov}}$
Mode VI	$V_{\mathrm{dc}} \le V_{\mathrm{ref}}^{\mathrm{batt}} - \Delta V^-$

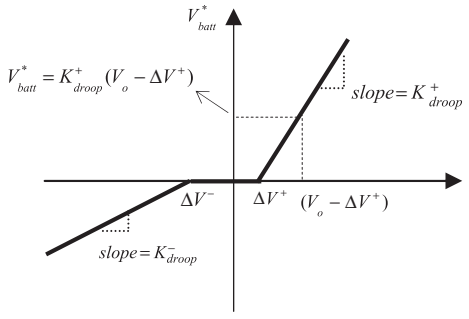

Fig. 13. DC bus voltage droop controller and power sharing implementation.

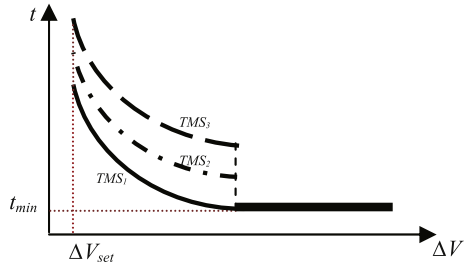

Fig. 14. Inverse time curve for load shedding implementation.

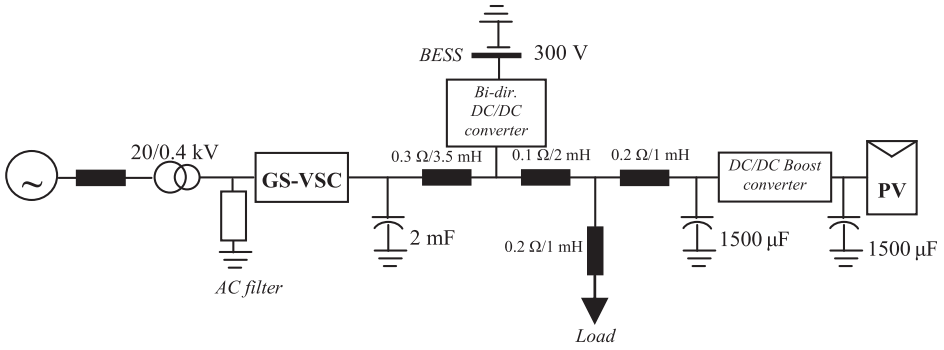

Fig. 15. Schematic diagram of the simulated DC micro-grid.

4. Power management strategy

Previous sections have described the control strategies for the PV and BESS. In a real grid, there may be multiple of such sources/storages dispersed throughout the grid thus; a power management scheme is needed to coordinate the sources/storages effectively. A distributed power management strategy using MDBS method is improved in this paper to maintain the power balance and stable operation of DC micro-grid under any generation or load conditions. In this approach DC bus voltage level change is utilized to communicate between sources and storages [28,38] and to recognize different operating modes according to the voltage levels defined in Table 2. The voltage thresholds are set as follows:

$V_{vsc} = 1.05$ pu reference voltage for the GS − VSC

$V_{ref}^{batt} = 1$ pu reference voltage for BESS

$\Delta V^{-} = -0.05$ pu reference voltage for the BESS to start discharging

$\Delta V^{+} = +0.02$ pu reference voltage for the BESS to start charging

$V_{grid}^{ov} = 1.1$ pu reference voltage for the PV to start in voltage control mode

$V_{shed} = 0.9$ pu reference voltage for the load shedding

When multiple of sources/storages are exist in the grid, each voltage range is divided into sub-ranges and sets the reference value for sources/storages in order to coordinates power sharing during different operating modes.

As discussed earlier, a load shedding scheme may also be necessary to protect the system against instability when the demanded power exceeds the maximum deliverable power. In this case, DC voltage cannot be fully controlled and will continue decreasing from the minimum allowable value. In order to prevent the total collapse of the DC micro-grid, a prioritized load shedding is implemented based on the local DC voltage measurement without the need for communication. Load shedding is performed by controlling the loads to shut down at different voltage levels as the bus voltage moves away from the desired value. A modified IEC standard inverse definite minimum time (IDMT) curve [39] shown in Fig. 14, is used for discrimination between loads according to their precedence for tripping. The trip voltage setting (ΔV_{set}) and the time multiply setting (TMS) is selected for each load in accordance with its priority. Critical loads will have a larger TMS or larger ΔV_{set}. This load shedding strategy provides two degree of freedom for loads to minimize the loss of load in the DC micro-grid. When load are near together, since they sense a relatively analogous voltage it may be better to discriminate the loads by the trip voltage setting [40]. A minimum time delay is also added to avoid load shedding in case of a transient voltage drop, e.g. a voltage sag on AC grid. However, when the loads are located in different places in the grid, they sense different voltage conditions depending on source/storage locations. Therefore, for a better protection of the DC grid against instability, load shedding strategies are coordinated using different TMS.

5. Case studies and simulation results

In order to validate the proposed control methods for distributed integration of PV and energy storage in a DC micro-grid, system simulations have been carried out using SIMULINK/

Table 3
Rating of the DC micro-grid elements.

DC micro-grid	Nominal voltage	400 V
	Cable parameters	Are shown on the diagram
GS-VSC	Power rating	5 kVA
	L_f, R_f, c_f	0.8 mH, 4 mΩ, 30 μF
Transformer	Nominal voltage	0.173/20 kV (L–L)
	Power rating	5 kVA
Total DC load	Constant resistance	80 Ω
	Constant power	4 KW
PV system	PV model parameters	[28] with $N_P = 3$, $N_S = 10$
	PV Boost converter switching frequency	5 kHz
	L, R_L, C, R_o, C_o, R_o	25 mH, 0.02 Ω, 1.5 mF, 0.02 Ω, 1.5 mF, 0.02 Ω
BESS	Type	Lead-acid
	Rating	300 V, 10 *A.h*
	Battery converter	5 kHz
	L, R_L, C, R_o, R_o	15 mH, 0.02 Ω, 1 mF, 0.025 Ω

Table 4
Operation events during Case1.

Time (s)	Operation event
1	Insolation reduces from 1000 to 900 W/m^2
2	Insolation reduces from 900 to 750 W/m^2
2.5	30% of total load is switched off
3	Insolation increases from 750 to 900 W/m^2
4	Insolation reduces from 900 to 800 W/m^2
5	Insolation reduces from 800 to 700 W/m^2
6	Insolation increases from 700 to 900 W/m^2
6.5	80% of total load is switched off
8	Insolation increases from 900 to 1000 W/m^2
8.5	15% of total load is switched on

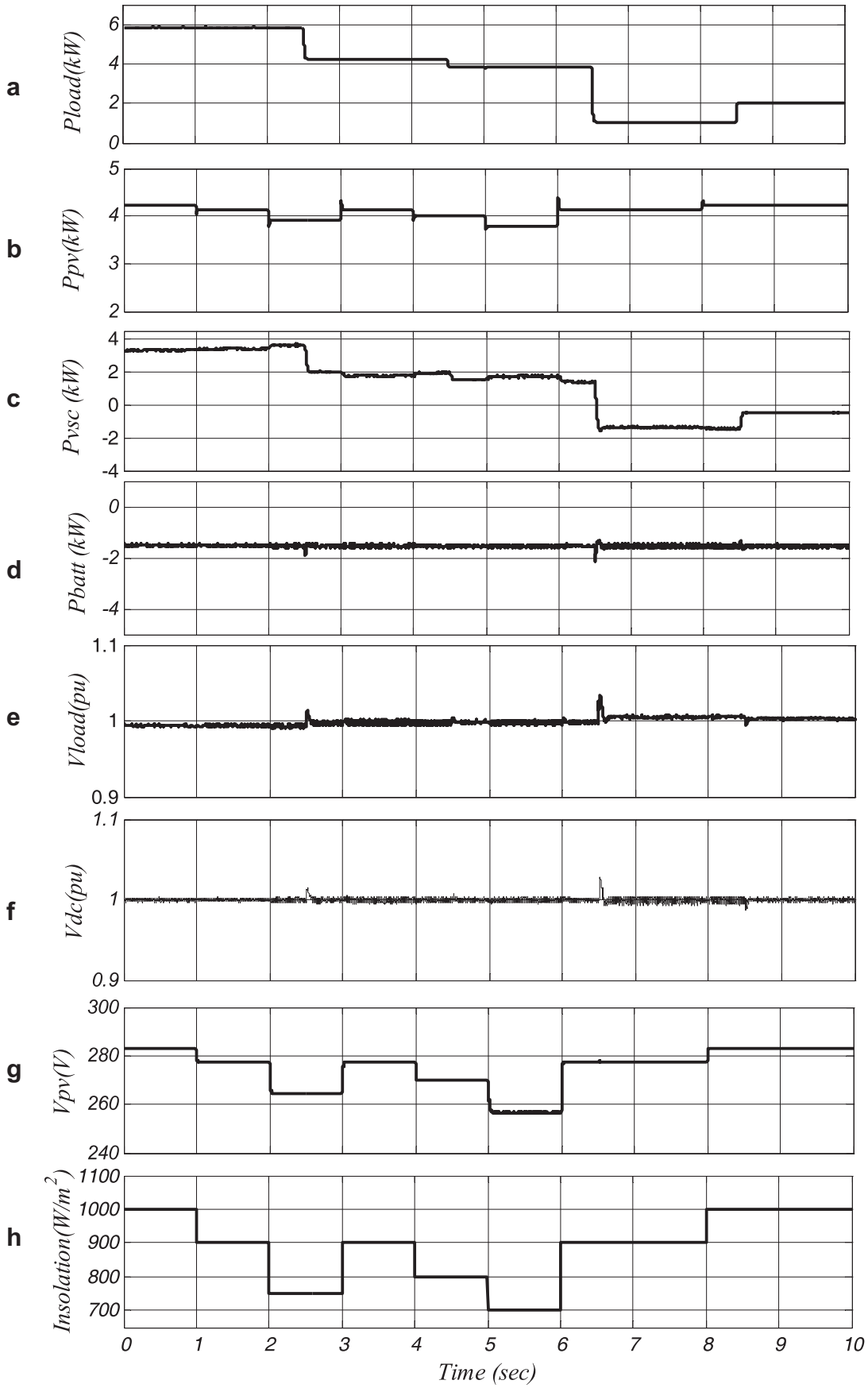

Fig. 16. System operation during load and PV generation variation in grid connected mode (Case1), (a) Total load (kW), (b) PV power generation (kW), (c) Power import/export by the GS-VSC (kW), (d) Battery charging power (kW), (e) DC voltage at load point, (f) DC-link voltage at GS-VSC (pu), (g) Solar insolation variation (W/m^2), (h) PV array voltage (Volts).

Table 5
Operation events during Case2.

Time (s)	Operation event
1	Transition to islanding mode
2	Insolation reduces from 1000 to 800 W/m^2
3.5	10% of initial load is switched on
5	Insolation increases from 800 to 900 W/m^2
6.5	10% of total load is switched off
7	Insolation increases from 900 to 1000 W/m^2
8.5	10% of initial load is switched off

Table 6
Operation events during Case3.

Time (s)	Operation event
1	Transition to islanding mode
2	Insolation reduces from 1000 to 800 W/m^2
3	Insolation increases from 800 to 1000 W/m^2
4	Insolation reduces from 1000 to 900 W/m^2
5	Insolation increases from 900 to 1000 W/m^2
6.5	5% of initial load is switched off

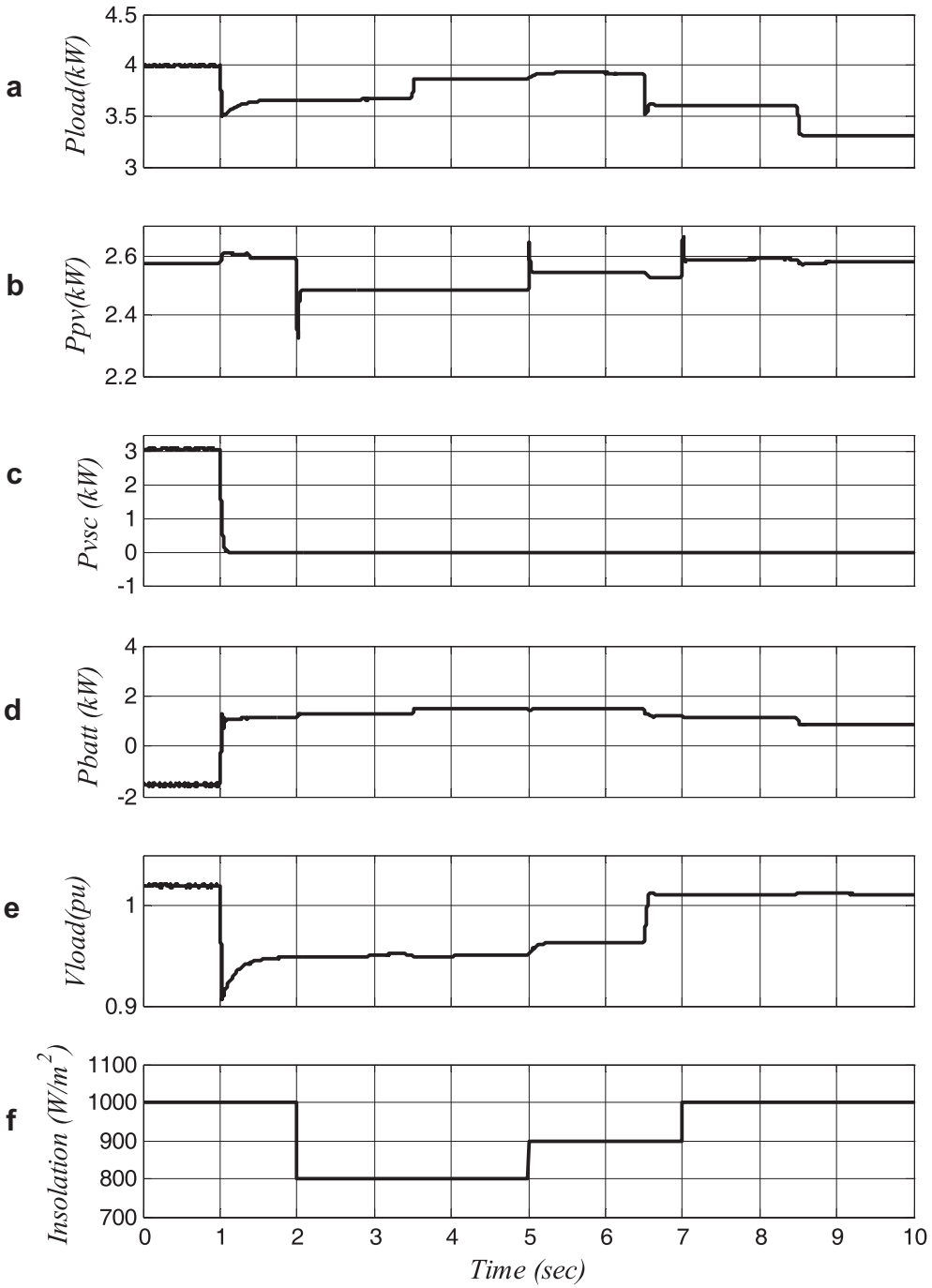

Fig. 17. System operation in transition to islanding (Case2), (a) Total load (kW), (b) PV power generation (kW), (c) Power of the GS-VSC (kW), (d) Battery charging/discharging power (kW), (e) DC voltage at load point, (f) Solar insdation variation (W/m^2).

MATLAB. A schematic diagram of the DC micro-grid is shown in Fig. 15 and the detailed ratings of the system elements are listed in Table 3. The following considerations are regarded for a stable operation of the system.

- Considering the nondeterministic characteristic of PV power generation and in order to ensure supply of DC load demand, the power rating of the GS-VSC is selected as the sum of maximum DC grid load demand and maximum charging power of batteries.
- The sum of maximum discharging power of batteries should be greater than the power of sensitive loads in the DC grid.
- The average power of PV array is also assumed to be equal to the sum of DC load power demand and battery charging power.

Based on the nominal PV converter model in the current source region and using the small signal model of the system, a second order lead compensator is designed as Equation (26) for the voltage control loop.

Table 7
Operation events during Case4.

Time (s)	Operation event
1	Transition to islanding mode
3	Insolation reduces from 1000 to 800 W/m^2
4.5	10% of total load is switched off
5	Insolation increases from 800 to 900 W/m^2
6.5	10% of total load is switched off
7	Insolation increases from 900 to 1000 W/m^2

$$G_{c\_pv} = 50\left(\frac{1+s/5884}{1+s/60318}\right)^2 \tag{26}$$

The same procedure is done for the battery loop compensator and a PI controller is designed as Equation (27),

$$G_{c\_b} = 20\left(1+\frac{10}{s}\right) \tag{27}$$

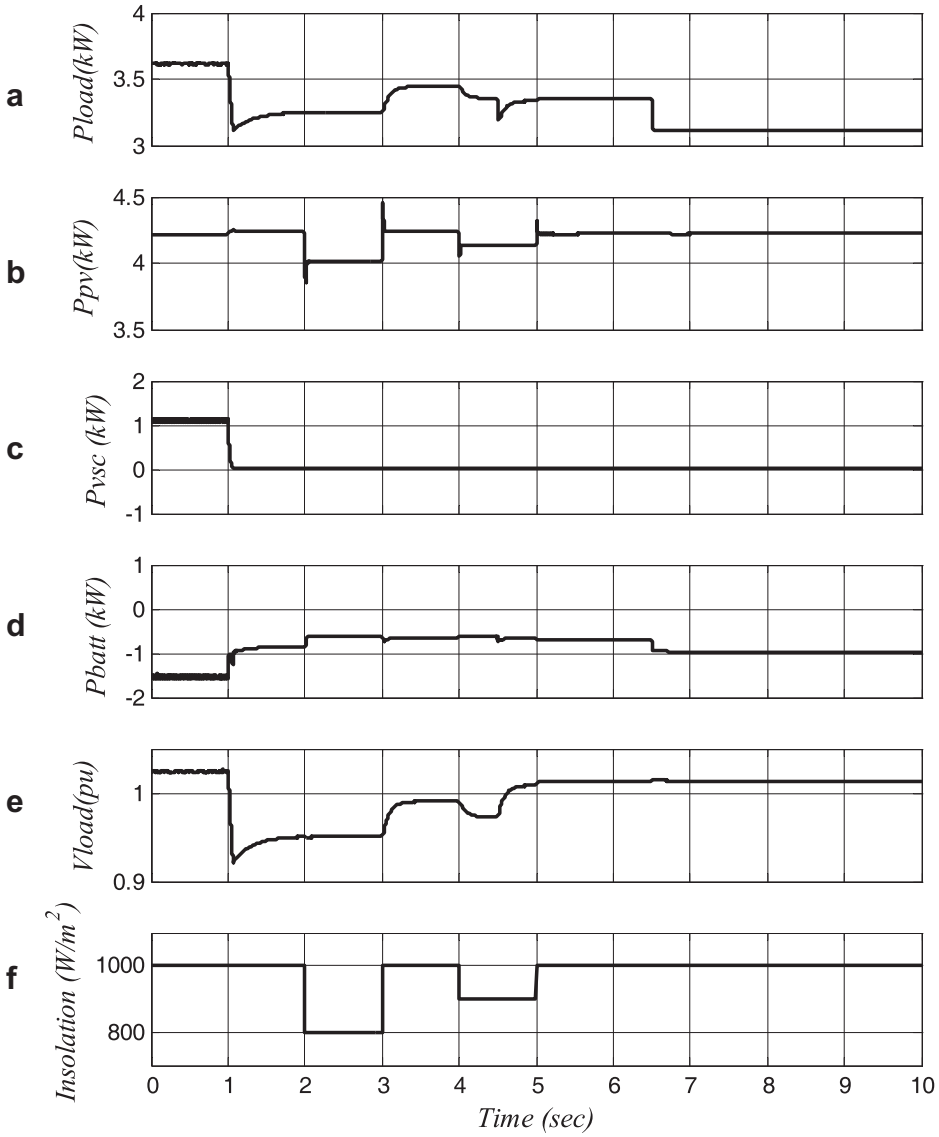

Fig. 18. System operation in transition to islanding (Case3), (a) Total load (kW), (b) PV power generation (kW), (c) Power of the GS-VSC (kW), (d) Battery charging/discharging power (kW), (e) DC voltage at load point, (f) Solar insolation variation (W/m^2).

Regarding the abovementioned conditions, different operating scenarios are simulated and the control methods to obtain a stable DC micro-grid are tested. The system is simulated for the two states of micro-grid i.e., grid connected and islanding and considers different operating modes and possible transition between these modes.

Different operating scenarios are simulated in order to validate the performance of the PV and BESS in controlling the DC voltage and supplying the load in the micro-grid. The scenarios and study cases are described in the following sections.

5.1. Case1

In this case, the DC micro-grid is supposed to be connected to an external AC micro-grid. At first, a portion of the demanded load is supplied by the PV and the insufficient power plus the battery charging power is provided by the GS-VSC by means of rectifying the AC power. During the simulation, the battery is charged in a constant power mode with nominal charging power, the GS-VSC is regulating the DC voltage and the PV is also working in MPPT mode. Effect of load and solar insolation variation are also considered in the simulation. At 6.5 s, a large portion of the DC load

Table 8
Operation events during Case5.

Time (s)	Operation event
1	Transition to islanding mode
1.2	A portion of load is shed in the first stage
1.5	A portion of load is shed in the second stage

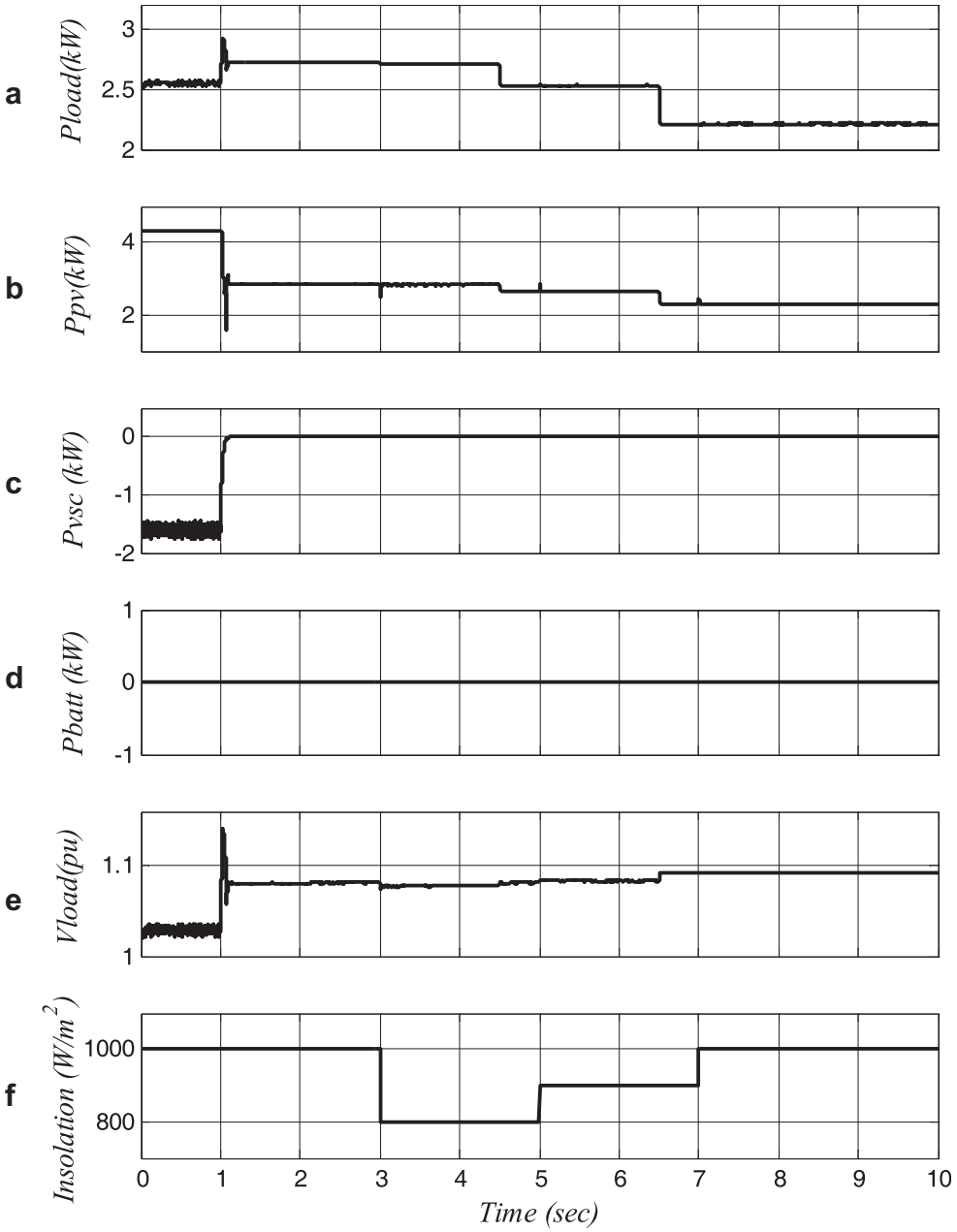

Fig. 19. System operation in transition to islanding (Case4), (a) Total load (kW), (b) PV power generation (kW), (c) Power of the GS-VSC (kW), (d) Battery power (kW), (e) DC voltage at load point, (f) Solar insolation variation (W/m^2).

switches off and the PV power generation is more than the load and battery charging power demand. The GS-VSC moves to inverting mode and the grid operates in Mode II. Operation events during this case are explained in Table 4. Load, GS-VSC, PV and battery power are illustrated in Fig. 16 (a)–(d), respectively. DC voltages at load point and at the DC-link of VSC are shown in Fig. 16 (e), (f), respectively. It can be concluded that the GS-VSC can smoothly regulate the DC-link voltage during different disturbances on DC micro-grid. Fig. 16 (g) also shows the PV array MPP voltage for different solar insolation levels shown in Fig. 16 (h).

5.2. Case2

This case simulates the transition from mode II to Mode III. This is related to the situation where the DC micro-grid moves into the islanding mode and isolates from the main AC grid at 1 s. It is supposed that PV power generation is less than the demanded load and the insufficient power is supplied by the GS-VSC before islanding. In this case, the BESS controls the DC voltage by discharging the battery energy. Effect of load and solar insolation variation are also considered in the simulation. For example, at

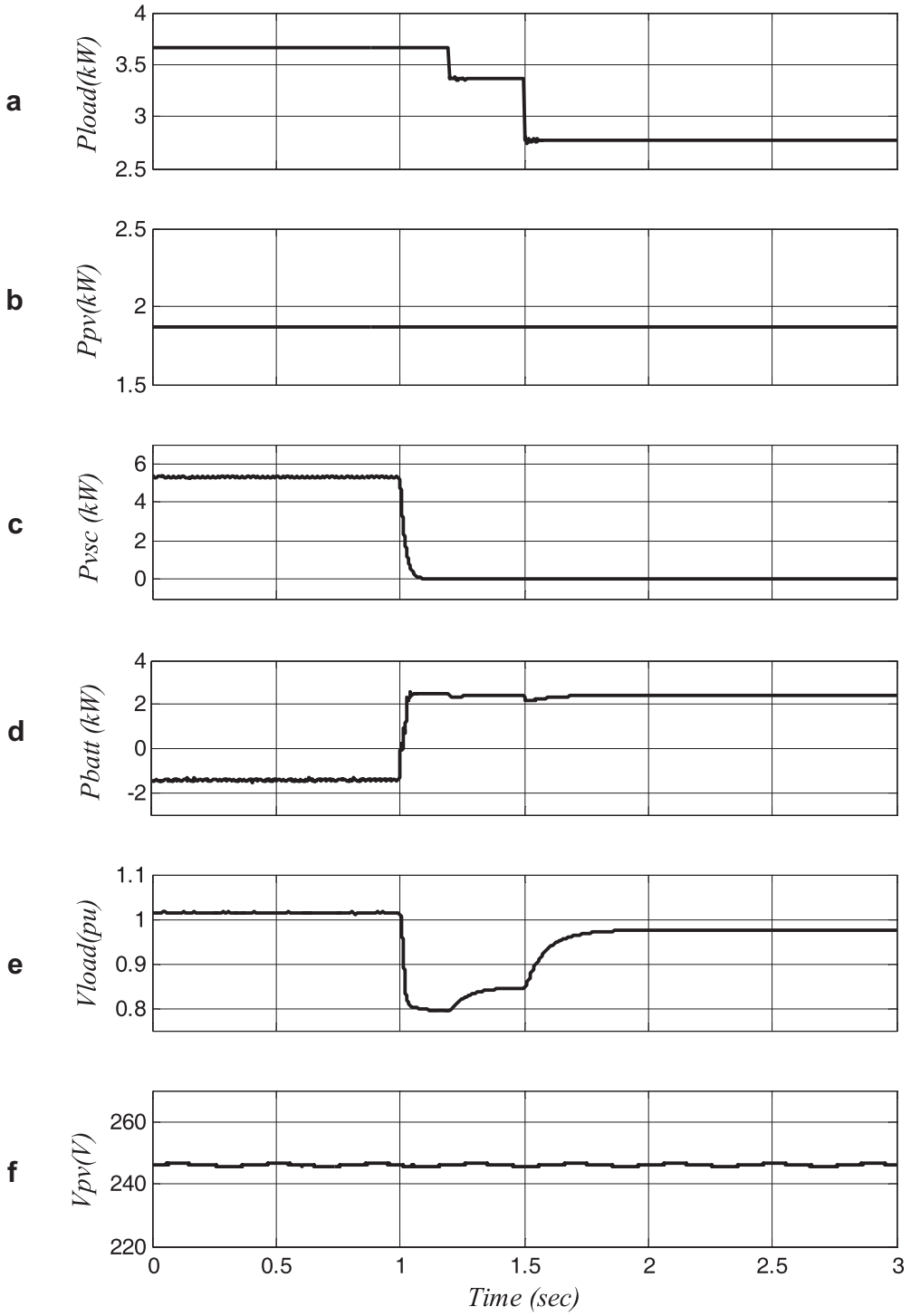

Fig. 20. System operation in transition to islanding (Case5), (a) Total load (kW), (b) PV power generation (kW), (c) Power of the GS-VSC (kW), (d) Battery charging/discharging power (kW), (e) DC voltage at load point, (f) PV array voltage (Volts).

3.5 s, load increases and the battery delivers more power to the DC grid and regulates the voltage as well. Operation events during this case are explained in Table 5. Simulation results are shown in Fig. 17. Load, GS-VSC, PV and battery power and DC voltage at load point are illustrated in Fig. 17 (a)–(e), respectively. It can be deduced that the BESS can control the DC voltage in islanding transition and smoothly regulate the voltage in case of load and solar insolation variations while the PV tracks the MPP during the simulation.

5.3. Case3

This case is similar to Case2 but, it is supposed that PV power is larger than the demanded load and the battery is not fully charged and simulates the transition from Mode I to Mode IV. In this case, the battery is partially charged in constant voltage mode and the BESS controls the DC voltage. Operation events during this case are explained in Table 6. Load, GS-VSC, PV, battery power and DC voltage at load point are illustrated in Fig. 18 (a)–(e), respectively. The effect of load and solar insolation variation on DC voltage, battery power and PV power is also considered in the simulation. It can be realized that the BESS can control the DC voltage in islanding transition and smoothly regulate the voltage in case of load and solar insolation variations while the PV tracks the MPP during the simulation.

5.4. Case4

This case deals with the case of transition from Mode I to Mode V. In this condition the battery is fully charged and the maximum generated power of the PV is greater than the demanded load. At 1 s, the micro-grid is islanded and the PV enters to the voltage control mode in order to regulate the DC voltage by controlling the output power. In this case, the PV works in off-MPPT mode and controls the DC voltage in the allowable voltage range and protects the system from overvoltage. The load and solar insolation variation is also considered in this case. It can be concluded that the control system can properly regulates the PV power generation and the DC voltage. Operation events during this case are explained in Table 7. Simulation results are shown in Fig. 19.

5.5. Case5

In this case, the load demand is greater than the total battery and PV power generation. The micro-grid is operating in Mode II before the islanding. At 1 s the micro-grid moves to islanding mode and since the generated power is less than the demanded load a voltage drop is caused in the DC grid which may cause instability because of the constant power loads that exist in the grid (Mode III). In order to operate the micro-grid stably, it is necessary to match generation and the load demand. The load shedding procedure is activated and switches off the less sensitive loads. At the first step a portion of load equal to 300 W is shut down and DC voltage increases but the voltage is still below the allowable range and the second load shedding step shuts down 600 W once more and the DC voltage recovers to the standard range. Operation events during this case are explained in Table 8. Simulation results are shown in Fig. 20.

6. Conclusion

This paper proposes a control strategy for distributed integration of PV and energy storage systems in a DC micro-grid including variable loads and solar radiation. The requirement of maintaining constant DC voltage is realized, considering different operating modes in grid connected and islanded states. The proposed control enables the maximum utilization of PV power during different operating conditions of the micro-grid and provides a smooth transfer between the grid connection and islanded mode. DC voltage levels are used as a communication link in order to coordinate the sources and storages in the system and acts as a control input for the operating mode switching during different operation conditions. System simulations have been carried out in order to validate the proposed control methods for the distributed integration of PV and energy storage in a DC micro-grid and the results show the reasonable operation of the micro-grid during various disturbances.

References

[1] Blaabjerg F, Zhe Chen, Kjaer SB. Power electronics as efficient interface in dispersed power generation systems. IEEE Trans Power Electron 2004;19(5):1184–94.
[2] Chakraborty S, Kramer B, Kroposki B. A review of power electronics interfaces for distributed energy systems towards achieving low-cost modular design. Renewable Sustainable Energy Rev 2009;13:2323–35.
[3] Salomonsson D, Sannino A. Low-voltage DC distribution system for commercial power systems with sensitive electronic load. IEEE Trans Power Delivery 2007;22(3):1620–7.
[4] Baran ME, Mahajan NR. DC distribution for industrial systems- opportunities and challenges. IEEE Trans Ind Appl 2003;39(6):1596–601.
[5] Kondratiev I, Dougal R. Synergetic Control Strategies for Shipboard DC Power Distribution Systems. In Proceedings of the 2007 American Control Conference. New York City, USA; July 11–13, 2007.
[6] Emadi Ali. Modeling and analysis of multiconverter DC power electronic systems using the generalized state-space averaging method. IEEE Trans Ind Electron 2004;51(3):661–8.
[7] Katiraei F, Iravani MR, Lehn PW. Micro-grid autonomous operation during and subsequent to islanding process. IEEE Trans Power Delivery 2005;20(1):248–56.
[8] Llaria A, Curea O, Jiménez J, Camblong H. Survey on microgrids: unplanned islanding and related inverter control techniques. Renewable Energy 2011;36:2052–61.
[9] Lopes JAP, Moreira CL, Madureira AG. Defining control strategies for microgrid s. IEEE Trans Power Syst 2006;21(2):916–24.
[10] Vandoorn Tine L, Meersman B, Degroote L, Renders B, Vandevelde L. A control strategy for islanded microgrids with DC-Link voltage control. IEEE Trans Power Delivery 2011;26(2):703–13.
[11] Kakigano Hiroaki, Miura Y, Ise T. Low-voltage bipolar-type DC micro-grid for super high quality distribution. IEEE Trans Power Electron 2010;25(12):3066–75.
[12] Karlsson P, Svensson J. DC Bus Voltage Control for Renewable Energy Distributed Power Systems. In Conf. Proc. Power and Energy Systems. Marina del Rey USA; May 2002.
[13] Lee Ji H, Kim HJ, Han BM, Jeong YS, Yang HS, Cha HJ, et al. DC micro-grid operational analysis with a detailed simulation model for distributed generation. J Power Electron 2011;11(3):350–9.
[14] Kurohane K, Uehara A, Senjyu T, Yona A, Urasaki N, Funabashi T, et al. Control strategy for a distributed DC power system with renewable energy. Renewable Energy 2011;36:42–9.
[15] Noroozian R, Abedi M, Gharehpetian GB, Hosseini SH. Combined operation of DC isolated distribution and PV systems for supplying unbalanced AC loads. Renewable Energy 2009;34:899–908.
[16] Sun X, Lian Z, Wang B, Li X. A hybrid renewable DC micro-grid voltage control. In: 6th conf. on power electronic and motion control. Wuhan: IPEMC; 2009. 17–20 May 2009.
[17] Amin M.M, Elshaer M.A, Mohammed O.A. DC Bus Voltage Control for PV Sources in a DC Distribution System Infrastructure. IEEE General Meeting on Power and Energy. 2010.
[18] Tofighi A, Kalantar M. Power management of PV/battery hybrid power source via passivity-based control. Renewable Energy 2011;36:2440–50.
[19] Xiong Liu, Wan P, Loh PC. Optimal Coordination Control for Stand-alone PV System with Nonlinear Load. In: IEEE international conf. on Power and Energy. ECCE; 2010.
[20] Chiang SJ, Shieh HJ, Chen MC. Modeling and control of PV charger system with SEPIC converter. IEEE Trans Ind Electronics 2009;56(11):4344–53.
[21] Koutroulis E, Kalaitzakis K. Novel battery charging regulation system for photovoltaic applications. IEE Proc-Electr Power Appl 2004;151(2):191–7.
[22] Katiraei F, Iravani MR. Power management strategies for a micro-grid with multiple distributed generation units. IEEE Trans Power Syst 2006;21(4):1821–31.
[23] Jiang Wei, Fahimi B. Active current sharing and source management in fuel cell–battery hybrid power system. IEEE Trans Ind Electronics 2010;57(2):752–61.
[24] Hajizadeh A, Golkar MA, Feliachi A. Voltage control and active power management of hybrid fuel-cell/energy-storage power conversion system

under unbalanced voltage sag conditions. IEEE Trans Energy Conversion 2010; 25(4):1195–208.
[25] Fakham Hicham, Lu Di, Francois Bruno. Power control design of a battery charger in a hybrid active PV generator for load-following applications. IEEE Trans Ind Electron 2011;58(1):85–94.
[26] Jiang Z, Gao L, Dougal RA. Adaptive control strategy for active power sharing in hybrid fuel cell/battery power sources. IEEE Trans Energy Convers 2007; 22(2):507–15.
[27] Zamora R, Srivastava AK. Controls for micro-grids with storage: review, challenges, and research needs. Renewable Sustainable Energy Rev 2010;14: 2009–18.
[28] Schönberger J, Duke R, Round SD. DC-bus signaling: a distributed control strategy for a hybrid renewable nanogrid. IEEE Trans Ind Electron 2006;53(5): 1453–60.
[29] Yazdani A, Rita Di Fazio A, Ghoddami H, Russo M, Kazerani M, Jatskevich J, et al. Modeling guidelines and a benchmark for power system simulation studies of three-phase single-stage photovoltaic systems. IEEE Trans Power Delivery 2011;26(2):1247–64.
[30] Ye L, Hai Bo Sun, Xu Ri Song, Li Cheng Li. Dynamic modeling of a hybrid wind/solar/hydro microgrid in EMTP/ATP. To be appeared in J Renewable Energy.
[31] Erickson RW. Fundamental of power electronics. Norwell, MA: Kluwer; 1997.
[32] Xiao W, Dunford WG, Palmer PR, Capel A. Regulation of photovoltaic voltage. IEEE Trans Ind Electron 2007;54(3):1365–74.
[33] Esram T, Chapman PL. Comparison of photovoltaic array maximum power point tracking techniques. IEEE Trans Energy Convers 2007;22(2):439–49.
[34] Durr M, Cruden A, Gair S, McDonald JR. Dynamic model of a lead acid battery for use in a domestic fuel cell system. J Power Sources 2006;161(2): 1400–11.
[35] Salameh ZM, Casacca MA, Lynch WA. A mathematical model for lead–acid batteries. IEEE Trans Energy Convers 1992;7(1):93–8.
[36] Barsali S, Ceraolo M. Dynamical models of lead–acid batteries: implementation issues. IEEE Trans Energy Convers 2002;17(1):16–23.
[37] Tremblay O, Dessaint LA, Dekkiche AI. A generic battery model for the dynamic simulation of hybrid electric vehicles. Proc IEEE Veh Power Propulsion Conf; 2007:284–9.
[38] Zhang L, Wu T, Xing Y, Sun K, Gurrero JM. Power control of DC microgrid using DC bus signaling. Appl Power Electron Conf Exposition (APEC); Mar. 2011:6–11.
[39] IEC 60255-3. Electric relays – part3: single input energizing quantity measuring relays with dependent or independent time; 1992.
[40] Tang W, Lasseter RH. An lvdc industrial power supply system without central control unit. Proc IEEE Power Electron Spec Conf 2000;2:979–84.